Available online at www.sciencedirect.com

SciVerse ScienceDirect

Ceramics International 38 (2012) 1051–1055

CERAMICS INTERNATIONAL

www.elsevier.com/locate/ceramint

Large-scale synthesis of WO_3 nanoplates by a microwave-hydrothermal method

Jarupat Sungpanich [a], Titipun Thongtem [b,c,*], Somchai Thongtem [a,c]

[a] Department of Physics and Materials Science, Faculty of Science, Chiang Mai University, Chiang Mai 50200, Thailand
[b] Department of Chemistry, Faculty of Science, Chiang Mai University, Chiang Mai 50200, Thailand
[c] Materials Science Research Center, Faculty of Science, Chiang Mai University, Chiang Mai 50200, Thailand

Received 27 July 2011; accepted 12 August 2011
Available online 19 August 2011

Abstract

Tungsten oxide (WO_3) nanoplates were synthesized by a 270 W microwave-hydrothermal reaction of $Na_2WO_4{\cdot}2H_2O$ and citric acid ($C_6H_8O_7{\cdot}H_2O$) in deionized water. X-ray diffraction (XRD), scanning electron microscopy (SEM), high resolution transmission electron microscopy (HRTEM), and selected area electron diffraction (SAED) were used to reveal the synthesis of WO_3 complete rectangular nanoplates in the solution of 0.2 g citric acid for 180 min, with O–W–O FTIR stretching modes at 819 and 741 cm^{-1}, and two prominent O–W–O Raman stretching modes at 804 and 713 cm^{-1}. The 2.71 eV indirect energy gap, and 430–460 nm blue emission wavelength range of WO_3 complete rectangular nanoplates were determined using UV–visible and photoluminescence (PL) spectrometers. The formation mechanism was also proposed according to the experimental results.

Keywords: B. Spectroscopy; B. X-ray methods; C. Optical properties; D. Transition metal oxides; Microwave-hydrothermal process

1. Introduction

At present, a great deal of effort has been focused on the nanostructured materials with zero-dimensional quantum dots, one-dimensional nanofibers, nanotubes and nanorods, and two-dimensional nanoplates and nanodisks, due to their novel properties. The unique photocatalytic and electrochromic properties of WO_3 [1,2] are generally well known for multiple potential applications, such as H_2S and NH_3 gas sensing [3,4], and electrochromic and photocatalytic materials [2]. For stoichiometric WO_3, tungsten ions have +6 valence oxidation state with the empty 5d shells. It is a distorted ReO_3 type, composed of corner and/or edge shared WO_6 octahedrons, caused by the 2nd order Jahn–Teller effect [1,5]. Tungsten oxide is an *n*-type indirect band gap (E_g) semiconductor with E_g of 2.5–2.9 eV [1,2], influenced by morphologies, crystalline degree, structural order–disorder, and synthetic methods.

In the present research, WO_3 nanoplates were synthesized by a microwave-hydrothermal method, without the use of any additives. This process is rapid and benign to the environment, and may lead to large-scale synthesis.

2. Experiment

In the present research, 0.3332 g $Na_2WO_4{\cdot}2H_2O$ and each of 0.1, 0.2, and 0.3 g citric acid ($C_6H_8O_7{\cdot}H_2O$) were dissolved in 40 ml deionized water, to form S1, S2, and S3 solutions. The pH of the solutions was adjusted to 1 using 37% HCl. Each of the solutions was transferred in lab-made autoclaves, which were tightly closed, and processed at 270 W microwave radiation for 30, 60, 90, 120, and 180 min. The final products were then characterized by different methods: X-ray diffractometer (XRD, SIEMENS D500, Germany) operating at 20 kV, 15 mA, and using Cu-K_α line, in combination with the database of the Joint Committee on Powder Diffraction Standards (JCPDS) [6]; scanning electron microscope (SEM, JEOL JSM-6335F, Japan) operating at 15 kV; transmission electron microscope (TEM, JEOL JEM-2010, Japan), high resolution transmission electron microscope (HRTEM) and selected area electron diffractometer

* Corresponding author at: Department of Chemistry, Faculty of Science, Chiang Mai University, Chiang Mai 50200, Thailand.
E-mail addresses: ttpthongtem@yahoo.com, ttpthongtem@gmail.com (T. Thongtem).

0272-8842/$36.00
doi:10.1016/j.ceramint.2011.08.030

(SAED) operating at 200 kV; Fourier transform infrared spectrometer (FTIR, Bruker Tensor 27, Germany) with KBr as a diluting agent and operated in the range of 4000–400 cm^{-1}; Raman spectrometer (T64000 HORIBA Jobin Yvon, U.S.A.) using a 50 mW and 514.5 nm wavelength Ar green laser; UV–visible spectrometer (Lambda 25 PerkinElmer, U.S.A) using a UV lamp with the resolution of 1 nm; and photoluminescence (PL) spectrometer (LS 50B PerkinElmer, U.S.A) using a 315 nm excitation wavelength at room temperature.

3. Results and discussion

3.1. XRD

Comparing XRD spectra (Fig. 1) of the products synthesized from S2 solution for 30, 60, 90, 120, and 180 min with the JCPDS database [6], they corresponded with pure monoclinic WO_3 (no. 72-1465) for 180 min long. When the processing time was shortened, mixed phases of monoclinic WO_3 and orthorhombic $WO_3{\cdot}H_2O$ (no. 84-0886) were detected [6].

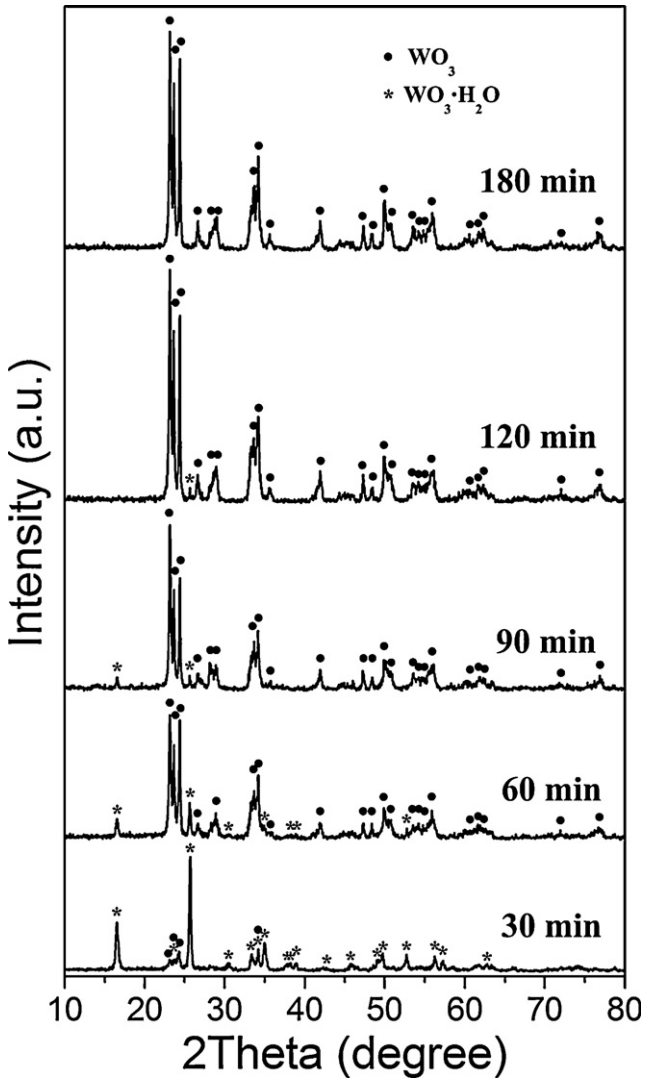

Fig. 1. XRD spectra of the products synthesized from S2 solution for different lengths of time.

3.2. SEM

SEM images of the products synthesized from different solutions and lengths of time are shown in Fig. 2. For the S2 solution and 30 min long (Fig. 2a), the product was irregular nanoplates with different orientations. Upon increasing the processing time from 30 min to 60, 90, 120, and 180 min (Fig. 2b–e) in sequence, they gradually transformed into rectangular nanoplates, and were complete for 180 min long. Upon varying the contents of citric acid (S1, S2, and S3 solutions) at the fixed processing time of 60 min (Fig. 2b, f and g), the product became complete rectangular nanoplates for using 0.3 g citric acid in the S3 solution. The present research proved that WO_3 morphologies were controlled by the lengths of time and contents of citric acid in the solutions.

3.3. SAED and HRTEM

SAED pattern (Fig. 3a) of the product synthesized from S2 solution for 180 min was indexed [7] to correspond with the (0 2 2), (0 0 2), (0 $\bar{2}$ 2), (0 2 0), (0 $\bar{2}$ 0), (0 2 $\bar{2}$), (0 0 $\bar{2}$) and (0 $\bar{2}$ $\bar{2}$) planes, specified as single crystalline WO_3 [6]. For the present analysis, electron beam was in the [1 0 0] direction. The (0 0 2) and (0 2 0) crystallographic planes with the respective 0.384 nm and 0.376 nm spaces at two positions were also detected in HRTEM images (Fig. 3b and c). These two planes were at right angle with each other – in accordance with the interpreted SAED pattern.

3.4. FTIR

FTIR spectra of the products synthesized from S2 solution for different lengths of time are showed in Fig. 4a. Obviously, the major vibrations associated with O–H stretching of residual water were detected at 3613–3134 cm^{-1}, C=O stretching modes at 1628 cm^{-1}, C–O stretching modes of carboxyl at 947 cm^{-1}, O–W–O stretching modes at 819 and 741 cm^{-1}, and W–O–W stretching modes at 659 cm^{-1} [5,8,9]. Upon increasing the processing time from 30 min to 60, 90, 120, and 180 min, the O–H and C=O stretching modes were gradually decreased and no longer detected for 180 min long. Still, a little of C–O stretching mode was detected.

3.5. Raman analysis

A definite existence of the products synthesized from S2 solution for different lengths of time was revealed by Raman spectra (Fig. 4b). Well-defined vibration modes centered at 804, 713, 610, 326, 275, 243, and 184 cm^{-1} were detected. Comparing Raman spectra of the present analysis and the WO_3 phase reported in the literatures [1,3,5,10–12], these products are monoclinic structure formed by O–W–O microcrystals connected with each other by W–O–W bonds, with the terminal W=O bonds at their surfaces. Two main peaks are typical O–W–O stretching modes of crystalline WO_3 at 804 cm^{-1} (symmetric) for the shorter bonds, and 713 cm^{-1} (asymmetric) for the longer bonds. Weak peaks at 610 cm^{-1} were assigned as the O–W–O stretching modes of WO_3

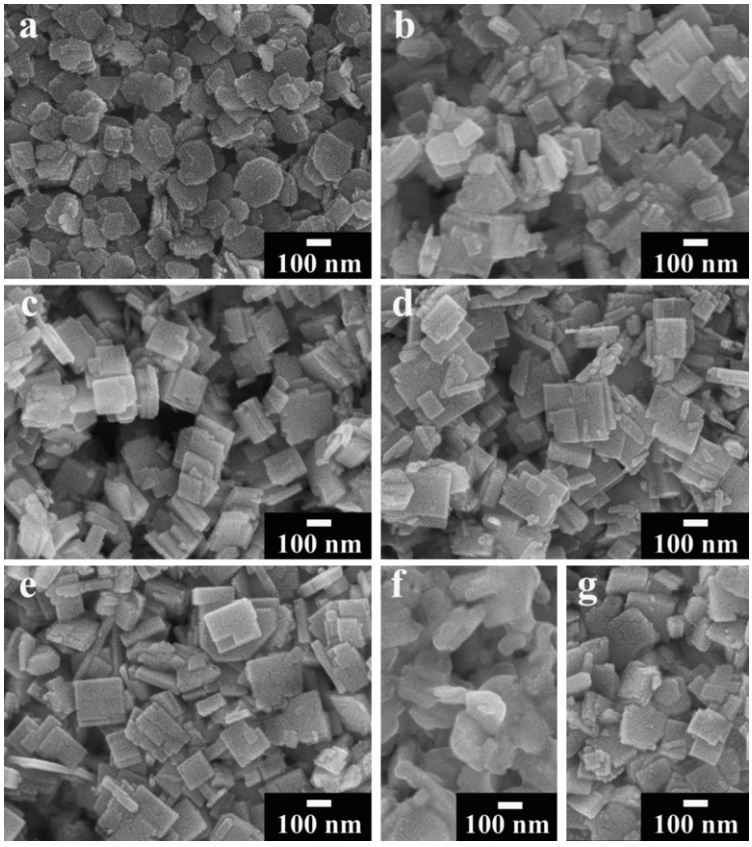

Fig. 2. SEM images of the products synthesized from (a–e) S2 solution for 30, 60, 90, 120, and 180 min, and (f and g) S1 and S3 solutions for 60 min, respectively.

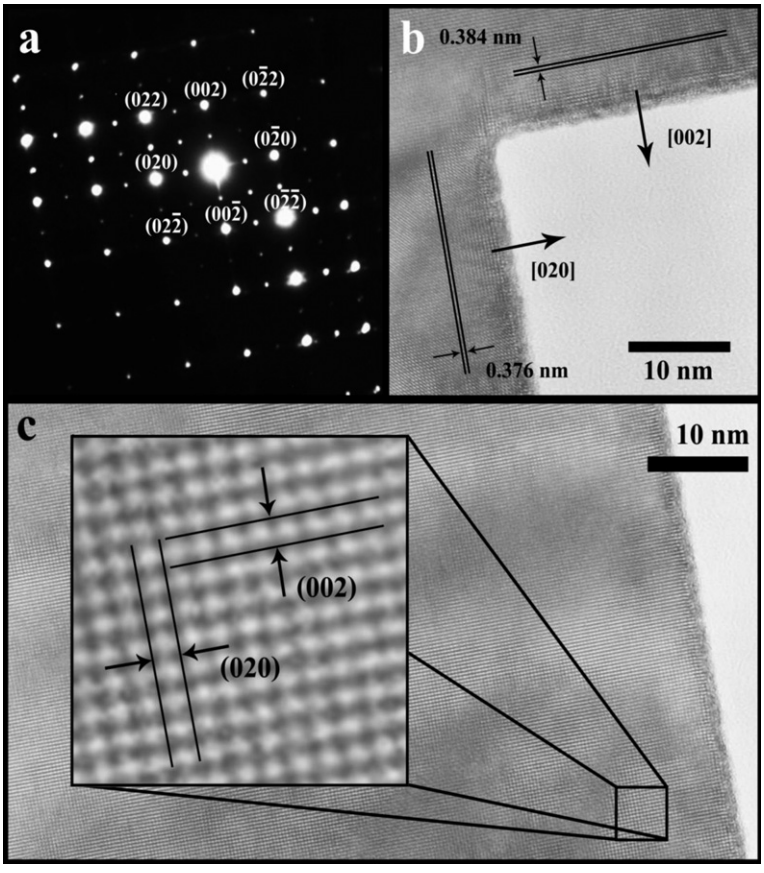

Fig. 3. (a) SAED pattern, and (b and c) HRTEM images of the product synthesized from S2 solution for 180 min.

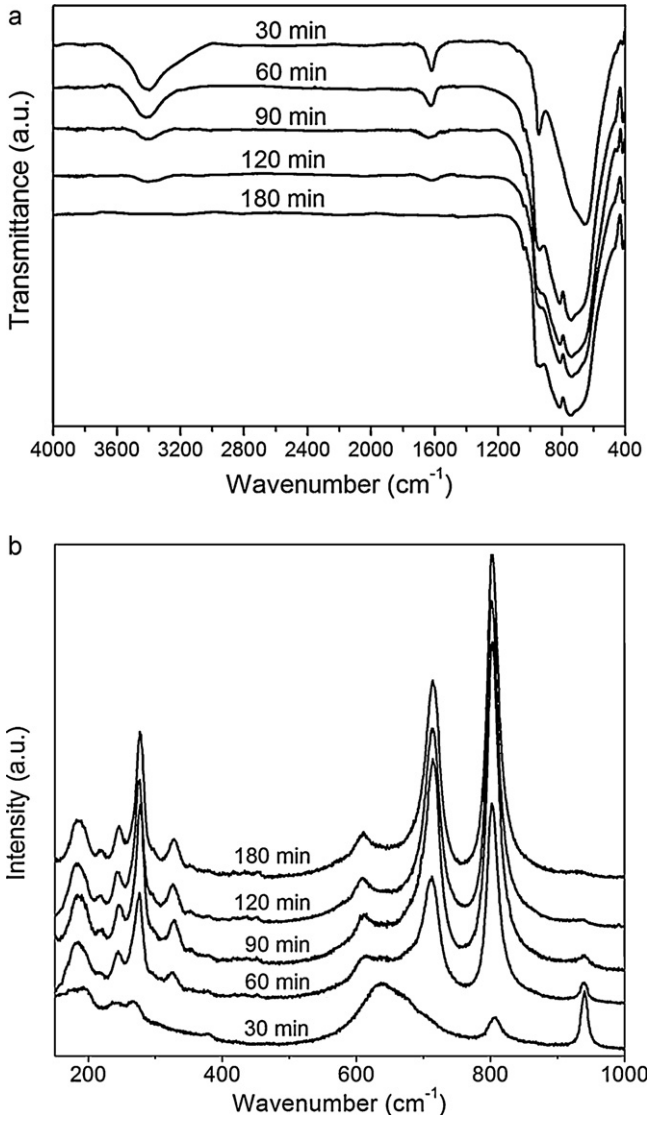

Fig. 4. (a) FTIR and (b) Raman spectra of the products synthesized from S2 solution for different lengths of time.

[5]. Those at 326, 275, and 243 cm^{-1} are assigned as W–O–W bending modes of the bridging oxide. The peak at 184 cm^{-1} is attributed to the lattice vibration of crystalline WO_3. Additional mode at 941 cm^{-1} belonging to W=O stretching [5] of the product processed for 30 min was detected. It was lessened for longer processing times, and no longer detected for 180 min long.

3.6. Proposed mechanism

During microwave-hydrothermal processing, $Na_2WO_4{\cdot}2H_2O$ reacted with citric acid ($C_6H_8O_7{\cdot}H_2O$) to form WO_3 molecules, which nucleated, and grew as WO_3 nanoplates.

$$2Na_2WO_4{\cdot}2H_2O + 2C_6H_8O_7{\cdot}H_2O \rightarrow 2WO_3 + 2C_6H_6O_7Na_2{\cdot}H_2O + 6H_2O \quad (1)$$

Initially, the nanoplates were irregular. They became rectangular and more complete, when the processing time was lengthened (Fig. 5). It should be noted that the nanoplates

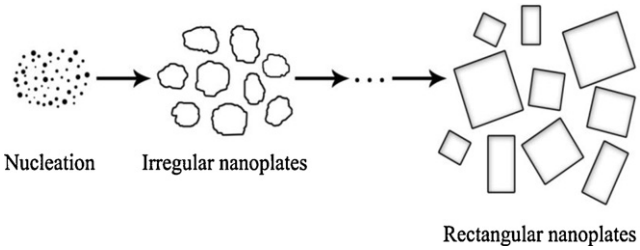

Fig. 5. Schematic diagram for the formation of rectangular nanoplates.

formed in different sizes, controlled by the initiation (born) of nuclei, aging time, growth rate, and surrounding concentration.

3.7. PL emission

The optical property (Fig. 6a) of WO_3 nanoplates synthesized from S2 and S3 solutions for different lengths of time was studied using 315 nm excitation wavelength. In this research, the emission peaks presented the bands over the 350–600 nm range with a strong blue emission peaks centered at the 430–460 nm wavelength range – in accordance with the reports of Wang et al. [2], and Lee et al. [13]. In the present research,

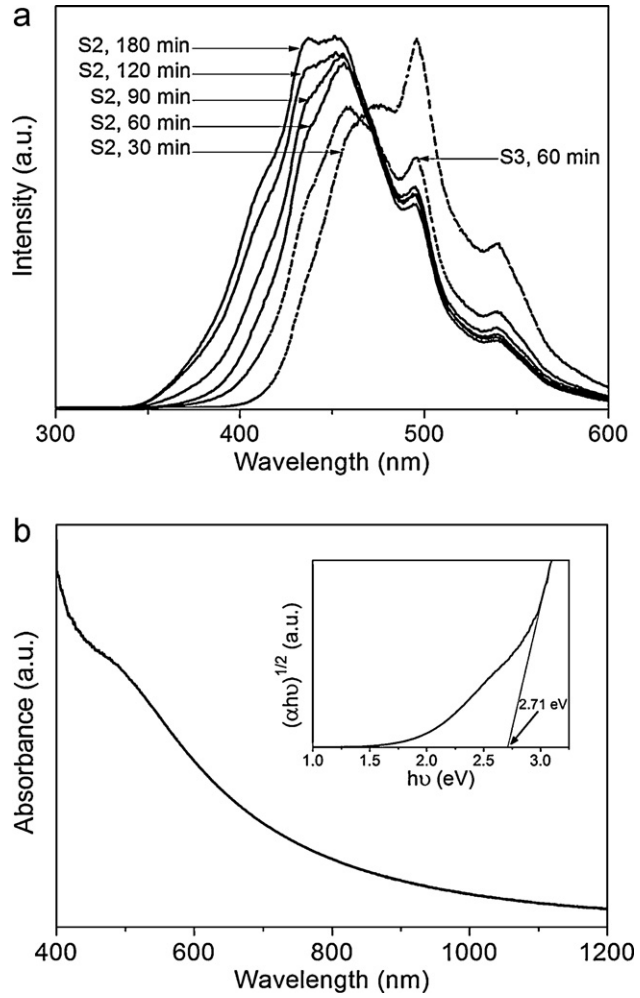

Fig. 6. (a) PL spectra of the products synthesized from S2 and S3 solutions for different lengths of time. (b) UV–visible absorption of the product synthesized from S2 solution for 180 min.

this PL emission was caused by electron–hole radiative recombination. Their shoulders were caused by localized states in the band gap due to impurities [13]. Some difference in the emission wavelengths was detected, caused by the phase, purity, morphologies, and synthesized conditions.

3.8. UV–visible absorption

UV–visible absorption (Fig. 6b) of the product synthesized from S2 solution for 180 min. By using Wood and Tauc equation [14] below.

$$\alpha h\nu = (h\nu - E_g)^n \quad (2)$$

where α is the absorbance, h is the Planck constant, ν is the photon frequency, E_g is the energy gap, and n is the pure numbers associated with the different types of charged transitions. For $n = 1/2$, 2, 3/2 and 3, the transitions are the direct allowed, indirect allowed, direct forbidden, and indirect forbidden, respectively. The absorption was controlled by two photon energy ($h\nu$) ranges relative to energy gap (E_g). For $h\nu > E_g$, absorption is linearly increased with the increasing of photon energy – caused by the transition of electrons from the topmost occupied state of valence band to the bottommost unoccupied state of conduction band. For $h\nu < E_g$, the absorption curve became different from linearity, caused by the charged transition relating to defects. In the present research, the indirect E_g was determined to be 2.71 eV (457.5 nm) – in accordance with the report of Kuzmin et al. [1], Wang et al. [2], and Su et al. [15]. It should be noted that this indirect E_g (457.5 nm) was in accordance with the 430–460 nm PL blue emission range as well.

4. Conclusions

WO_3 nanoplates were successfully synthesized by microwave-hydrothermal reaction of $Na_2WO_4{\cdot}2H_2O$ and citric acid ($C_6H_8O_7{\cdot}H_2O$) in deionized water for different lengths of time. By increasing the processing time of the 0.2 g citric acid solution to be 180 min, the product became pure monoclinic WO_3 with complete rectangular nanoplates. The indirect energy gap was determined to be 2.71 eV, and photoemission to be 430–460 nm wavelength range.

Acknowledgements

We wish to thank the National Nanotechnology Center (NANOTEC), National Science and Technology Development Agency (NSTDA), Thailand, for providing financial support through the project code: P-10-11345 for Research, Development and Engineering (RD&E), the Thailand's Office of the Higher Education Commission through the National Research University (NRU) Project, and the Thailand Research Fund (TRF) through the Royal Golden Jubilee Ph.D. Program, including the Graduate School of Chiang Mai University for general support.

References

[1] A. Kuzmin, J. Purans, E. Cazzanelli, C. Vinegoni, G. Mariotto, X-ray diffraction, extended x-ray absorption fine structure and Raman spectroscopy studies of WO_3 powders and $(1-x)WO_{3-y}{\cdot}xReO_2$ mixtures, J. Appl. Phys. 84 (1998) 5515–5524.
[2] J. Wang, P.S. Lee, J. Ma, Synthesis, growth mechanism and room-temperature blue luminescence emission of uniform WO_3 nanosheets with W as starting material, J. Cryst. Growth 311 (2009) 316–319.
[3] C.S. Rout, M. Hegde, C.N.R. Rao, H_2S sensors based on tungsten oxide nanostructures, Sens. Actuators B 128 (2008) 488–493.
[4] J. Leng, X. Xu, N. Lv, H. Fan, T. Zhang, Synthesis and gas-sensing characteristics of WO_3 nanofibers via electrospinning, J. Colloid Interface Sci. 356 (2011) 54–57.
[5] B. Ingham, S.V. Chong, J.L. Tallon, Layered tungsten oxide-based organic-inorganic hybrid materials: An infrared and Raman study, J. Phys. Chem. B 109 (2005) 4936–4940.
[6] Powder Diffract. File, JCPDS-ICDD, 12 Campus Boulevard, Newtown Square, PA 19073-3273, USA, 2001.
[7] K.W. Andrews, D.J. Dyson, S.R. Keown, Interpreting Electron Diffraction Patterns, Plenum Press, New York, 1971.
[8] H.S. Mansur, C.M. Sadahira, A.N. Souza, A.A.P. Mansur, FTIR spectroscopy characterization of poly (vinyl alcohol) hydrogel with different hydrolysis degree and chemically crosslinked with glutaraldehyde, Mater. Sci. Eng. C 28 (2008) 539–548.
[9] H.S. Mansur, R.L. Oréfice, A.A.P. Mansur, Characterization of poly(vinyl alcohol)/poly(ethylene glycol) hydrogels and PVA-derived hybrids by small-angle X-ray scattering and FTIR spectroscopy, Polymer 45 (2004) 7193–7202.
[10] S. Salmaoui, F. Sediri, N. Gharbi, Characterization of h-WO_3 nanorods synthesized by hydrothermal process, Polyhedron 29 (2010) 1771–1775.
[11] T. Siciliano, A. Tepore, G. Micocci, A. Serra, D. Manno, E. Filippo, WO_3 gas sensors prepared by thermal oxidization of tungsten, Sens. Actuators B 133 (2008) 321–326.
[12] Y.S. Kim, Thermal treatment effects on the material and gas-sensing properties of room-temperature tungsten oxide nanorod sensors, Sens. Actuators B 137 (2009) 297–304.
[13] K. Lee, W.S. Seo, J.T. Park, Synthesis and optical properties of colloidal tungsten oxide nanorods, J. Am. Chem. Soc. 125 (2003) 3408–3409.
[14] S. Wannapop, T. Thongtem, S. Thongtem, Characterization of $SrWO_4$–PVA and $SrWO_4$ spiders' webs synthesized by electrospinning, Ceram. Int. (2011), doi:10.1016/j.ceramint.2011.06.005.
[15] X. Su, F. Xiao, Y. Li, J. Jian, Q. Sun, J. Wang, Synthesis of uniform WO_3 square nanoplates via an organic acid-assisted hydrothermal process, Mater. Lett. 64 (2010) 1232–1234.